# Interplay between H-bonding proton dynamics and Fe valence fluctuations in Fe 3 ( P O 4 ) 2 ( OH ) 2 at high pressure

G. Hearne, V. Ranieri, P. Hermet, J. Haines, O. Cambon, J. Bantignies, P. Fertey, T. Stuerzer, M. Poienar, J. Rouquette

(text incl footnotes 3444 w, figures 549 w, figure captions 481w: **total 4475 w**)

ver25 resubmit

# Interplay between H-bonding proton dynamics and Fe valence fluctuations in $Fe_3(PO_4)_2(OH)_2$ at high pressure


G. Hearne[1*], V. Ranieri[2], P. Hermet[2], J. Haines[2], O. Cambon[2], J.L. Bantignies[3], P. Fertey[4], T. Stuerzer[5], M. Poienar[6], J. Rouquette[2*]

[1]Department of Physics, University of Johannesburg PO Box 524, Auckland Park 2006, Johannesburg, South Africa

[2]ICGM, Université de Montpellier, CNRS, ENSCM, 34095 Montpellier, France

[3]L2C, Université de Montpellier, CNRS, 34095 Montpellier, France

[4]Synchrotron Soleil, L'Orme des Merisiers, Saint-Aubin, BP 48, 91192 Gif-sur-Yvette Cedex, France

[5]Bruker AXS GmbH, Ostliche Rheinbruckenstrasse 49, Karlsruhe D-76187, Germany

[6]National Institute for Research and Development in Electrochemistry and Condensed Matter (INCEMC), Renewable Energies - Photovoltaic Laboratory (LERF), Str. Dr. A. Paunescu Podeanu, nr.144, 300569, Timisoara, Timis, Romania

[*] Corresponding authors: grhearne@uj.ac.za ; jerome.rouquette@umontpellier.fr

(text incl footnotes 3444 w, figures 549 w, figure captions 481w: **total 4475 w**)


## Abstract

We pressure tune the hydrogen bond in Fe-O–H···O-P structural segments of mixed-valence barbosalite $(Fe^{2+}Fe^{3+}_2)(PO_4)_2(OH)_2$. Infrared spectroscopy evidences changes in softening of O–H stretch modes and excessive profile broadening onset below 10 GPa. Single-crystal X-ray diffraction shows pseudo-symmetrization of the original monoclinic unit cell concurs with these changes in the O–H vibrational mode. These are considered compelling indicators of proton delocalization onset below 10 GPa as hydrogen bonds are strengthened under pressure. Subsequently in the range 10–30 GPa, Fe Mössbauer spectroscopy discerns $Fe^{2+} \Leftrightarrow Fe^{3+}$ valence fluctuations at proximate cations of the hydrogen bonds. When the original crystal potential at an $Fe^{2+}$ site is perturbed by proton delocalization at a ligand, electron exchange is induced along $Fe^{2+} \rightarrow L \rightarrow Fe^{3+}$ pathways (ligand $L$ = O or $(OH)^-$ of shared octahedral faces). Thus, $(Fe^{2+}Fe^{3+}_2)(PO_4)_2(OH)_2$ under pressure exemplifies the interplay between proton (THz) and electron (MHz) dynamics on two disparate time scales in the same condensed phase.

(text incl footnotes 3444 w, figures 549 w, figure captions 481w: **total 4475 w**)

*Introduction.* There is considerable interest in iron hydroxyl phosphates, which occur in various mineral forms and are readily synthesised by hydrothermal methods. They are used as catalysts in methyl methacrylate synthesis, of importance in polymer manufacturing [1]. They are also candidates for positive-electrode materials in Li-ion rechargeable batteries, in analogy to the well-known phospho-olivine $LiFePO_4$ [2]. These important applications potentially arise from the coexistence of two intrinsic physical properties in these compounds: iron mixed-valence state and the occurrence of hydrogen bonds in lattice segments, e.g., in barbosalite $(Fe^{2+}Fe^{3+}{}_2)(PO_4)_2(OH)_2$.

Mixed-valence barbosalite $Fe^{2+}Fe^{3+}{}_2(PO_4)_2(OH)_2$ has a six-fold coordination of Fe involving $FeO_4(OH)_2$ octahedra, each of which have $(OH)^-$ hydroxyl groups in a *trans* configuration [3]. Such $(OH)^-$ intermediaries form part of Fe-O–H···O-P structural sequences involving hydrogen bonds and a double-well proton potential energy profile along the line of oxygens [4]. Pressurizing such mixed-valence iron hydroxy phosphates affords a unique opportunity for investigating how changes in O–H···O hydrogen bonding may influence $Fe^{2+} \rightarrow (OH)^- \rightarrow Fe^{3+}$ inter-valence electron transfer, and vice-versa. Such an interplay between proton and *d*-electron dynamics is also expected to impact on magnetic properties, as demonstrated in the topical quantum spin liquid candidate $H_3LiIr_2O_6$ [5].

Controlled reductions of barbosalite's unit-cell volume by applied pressure will reduce O···O distances in O–H···O hydrogen bonds. This tunes the original double-well potential involving proton localization in one of the minima, to have a low enough barrier across which proton delocalization occurs via quantum tunnelling [4-6]. Further reductions in O···O distances may lead to symmetrisation of the hydrogen bond where the proton locates at the centre between the oxygens, in a pronounced anharmonic single-minimum potential [7].

The relevance of this, for example, is that nominally anhydrous minerals are a major source of $H_2O$ in planetary interiors, in the form of hydroxyl groups $(OH)^-$ incorporated in the polyhedral coordination of cations in these structures. The thermoelastic moduli of these mantle minerals and the impact on seismic behaviour are influenced by these O–H···O configurations, notably degree of O–H···O asymmetry or whether symmetrisation has occurred under extreme pressure-temperature conditions [8].

We have pressurised monoclinic barbosalite $Fe^{2+}Fe^{3+}{}_2(PO_4)_2(OH)_2$ in diamond-anvil cells (DACs) up to ~30 GPa at room temperature (RT). We deploy single-crystal X-ray diffraction (SC-XRD) and infrared (IR) spectroscopy to monitor unit-cell evolution and proton state *in situ*, respectively, as O–H···O bonds evolve under pressure [6c]. $^{57}$Fe Mössbauer spectroscopy

(MS) is used to discern the Fe local atomic environment, as a complementary and direct probe of cations proximate to pressure-tuned hydrogen bonds [9]. Methodological details are in the Supplemental Material (SM) [10].

Our pressure study of mixed-valence barbosalite follows on from previous interesting findings of the interplay between single Fe-valence perturbations and proton dynamics of hydrogen bonds in some inorganic assemblages. For example, in layered brucite-type $Fe(OH_2)$ [11], pressurisation leads to increased interaction amongst protons in the hydrogen bonds. The resultant breakdown of O-H axial symmetry creates an effective dipole potential at the iron site. This, in addition to the relatively weak binding energy of the minority-spin valence electron, triggers "self-oxidation" $Fe^{2+} \rightarrow Fe^{3+} + e^-$, onset at some cation sites at ~8 GPa and progresses with ever increasing abundance up to ~40 GPa.

*Structural considerations.* Our SC-XRD studies indicate barbosalite crystallizes in the monoclinic space group $P2_1/n$ at ambient conditions. Alternating $Fe^{2+}$ and $Fe^{3+}$ octahedra sharing opposite faces, form infinite chains in <110> directions, depicted in Fig. 1(a). A typical charge-ordered sequence in a chain is …–*V*–$Fe^{3+}$–$Fe^{2+}$–$Fe^{3+}$–*V*–$Fe^{3+}$–*V*–$Fe^{2+}$–$Fe^{3+}$–$Fe^{3+}$ … where *V* represents disordered vacant octahedral sites, due to some low occupancy of Fe in the vacant octahedral locations separating trimer sequences in Fig. 1(a). Further renditions and details of the structure are in Sub-sect. S1.1.2 of the SM [10], see Fig. S5. A hydrogen bond O–H···O forms between the $(OH)^-$ common vertex of mainly three (and sometimes four) octahedra and one of the oxygens involving a $PO_4$ group, i.e., as part of Fe-O–H···O-P segments of the lattice structure. At ambient conditions hydrogen bonds are asymmetric involving double-well proton potential energy profiles along the line of oxygens [5, 6d]. Proton configurations in O–H···O bonds throughout the structure are likely to be ordered in one of the potential energy minima of a slightly asymmetric double-well potential, due to repulsive effects of proton next-nearest neighbour $Fe^{2+}$ and $Fe^{3+}$ cations.

*Results and discussion.* At $P \geq 5$ GPa, SC-XRD results in Fig. 1(b) indicate a conspicuous pseudo-symmetrization of original disparate lattice parameters of the monoclinic unit-cell. Although, the volume does not show a discernible discontinuity in this regime. Additionally, the hydrogen bond in Fe-O–H···O-P structural sequences up to ~16 GPa is monitored via the IR-active O–H bond stretching vibration [6c, 12], in Fig. 1(c). Note, even at ambient pressure these hydrogen bonds are near to moderate strength [4], deduced from IR stretch frequencies lower than the ~3500 $cm^{-1}$ typical of weak hydrogen bonds. Fig. 1(d) depicts the pressure evolution of O–H symmetric and asymmetric stretch mode frequencies and their average

frequency, up to where the two stretch modes are visibly resolved at 5–6 GPa [11b]. Thereafter, excessive mode broadening occurs and the frequency is taken as the extremum value of the broad maximum. There is a weak negative pressure dependence of the average O–H stretch-mode frequency up to ~4 GPa. Then a change to a much steeper negative pressure dependence occurs up to ~7 GPa, after which there is a change to a different negative pressure dependence and appreciable line broadening is evident. By 8–10 GPa O–H stretch modes manifest as a broadened humped profile.

The negative pressure dependence of the average O–H stretch-mode frequency (softening behaviour) and steep change in pressure dependence at ~4 GPa, indicate entry into the intermediate- or moderate-strength hydrogen bond regime [4, 6c]. The steep pressure dependence of the O–H stretch frequency and excessive line broadening at ~7 GPa and beyond can be rationalized by proton delocalization (dynamical hydrogen disorder) involving an IR excited vibrational state [6c, 12], i.e., from an $E_0 \rightarrow E_2$ transition in the inset of Fig. 1(d) [13]. Further pressurization to $P > 7$ GPa continues to lower the energy barrier. This leads to an increased likelihood of proton delocalization in the ground state, by way of quantum tunnelling [6c, 6d], across a low-barrier potential along the line of oxygens in Fe-O–H···O-P structural sequences of Fig 1(a). This manifests, on the scale of the proton potential-energy barrier height, as a discernible tunnel splitting of zero-point vibrational energy states $E_0$ and $E_1$ in the inset of Fig. 1(d) [5], and as proton tunnelling frequencies on an experimentally determinable timescale.

Entry into the regime of incipient proton delocalization at 4–7 GPa also manifests in the pseudo-symmetrization of lattice parameters in Fig. 1(b). This involves a *P21/n* → *Cc* displacive phase transition, wherein <110> octahedral chains similar to Fig 1(a) are maintained but with *a* and *b* axes doubling in the unit-cell, delineated in Sub-sect. S1.2 of the SM [10].

The onset of such proton dynamics at 4–7 GPa, as part of the surrounding charge environment of the cations, alters the crystal field potential at the Fe sites. This crystal field potential initially had partly a dipole field contribution from the polar O–H intramolecular bond and contributions from other oxygens in the $FeO_4(OH)_2$ octahedral local environment. We then examine what are the physical effects of hydrogen bond reinforcement in Fe-O–H···O-P structural segments, at longer ranges beyond the oxygen endpoints, i.e., at the cations. To this end, we deployed $^{57}$Fe MS to directly probe the proximate cations under pressure, viz., Fe charge state and local atomic environment, from behaviour of the hyperfine interaction (HI) parameters [9, 14], see also Sec. S4 of the SM [10].

(text incl footnotes 3444 w, figures 549 w, figure captions 481w: **total 4475 w**)

Evolution of $^{57}$Fe MS spectral profiles of $Fe^{2+}Fe^{3+}{}_2(PO_4)_2(OH)_2$ under pressure up to ~30 GPa are shown in Fig. 2(a). At the lowest pressure notice the conspicuous signature $Fe^{2+}$ wide quadrupole splitting (QS, doublet) and large isomer shift (IS, centroid) values, compared with $Fe^{3+}$ signatures in the near-central zero-velocity region. $Fe^{2+}$ signatures show noticeable changes at $P \geq 10$ GPa, manifested as progressively increasing line broadening and asymmetry, and reductions in resonance intensity. Less conspicuous changes occur in the $Fe^{3+}$ component, because some of the more abundant $Fe^{3+}$ sites are likely not influenced by whatever is causing electronic changes at $Fe^{2+}$ sites.

Spectral evolution in Fig. 2(a) is typical of a low pressure charge-ordered state progressing to a $Fe^{2+} \Leftrightarrow Fe^{3+}$ valence fluctuation regime at higher pressures; also suggested by the dynamical theory fitting in Fig. 2(b) and simulations in Fig. S11 [10]. HI parameters initially fall in well-known characteristic ranges for static charge-ordered situations of $Fe^{2+}$ and $Fe^{3+}$ [15]. Whereas Fig. S11 simulations indicate HI parameters IS and QS of the spectral profile appear to be weighted average values of the static situation when fast valence fluctuations occur at an Fe site [9, 16], $Fe^{2+} \Leftrightarrow Fe^{3+}$, for example from inter-valence electron transfer $Fe^{2+} \rightarrow Fe^{3+}$ across face-sharing octahedra. This is where the fast relaxation time $\tau_R$ between two valence states is much shorter than the $^{57}$Fe nuclear quadrupole precession time, $\tau_Q$ ~40 ns [17], in the electric field gradient (EFG) from surrounding aspherical distributions of electronic and lattice charges. Motional narrowing of spectral profiles ensue in this case of $\tau_R \ll \tau_Q$. When $\tau_R \sim \tau_Q$, spectral profiles develop smeared out (broadened) features where distinct valence signatures are not readily discerned [16, 18]. The dynamical theory fitting exemplifies this in Fig. 2(b) [16, 19], where slow relaxation $\tau_R \gg \tau_Q$ and evolution at the highest pressures toward the intermediate relaxation time regime $\tau_R \sim \tau_Q$ are depicted. In all cases the 2:1 $Fe^{3+}$:$Fe^{2+}$ original stoichiometry for barborsalite is taken into consideration. Spectral line shapes when $\tau_R$ is within a 1–1000 ns time window yield quantitative information on the valence state (electron) dynamics, as exemplified in Fig. S11 simulations [10]. Therefore, pressure evolution of spectra in Fig. 2 signify a change from a slow relaxation (static) case tending to a regime of intermediate relaxation times of Fe valence fluctuations.

$Fe^{2+} \Leftrightarrow Fe^{3+}$ valence fluctuations at high pressure and associated 3*d* electron configuration changes $t_{2g}{}^4e_g{}^2(\uparrow\downarrow\uparrow\uparrow)(\uparrow\uparrow) \Leftrightarrow t_{2g}{}^3e_g{}^2(\uparrow\uparrow\uparrow)(\uparrow\uparrow)$, suggested by Fig. 2, are plausibly a result of $t_{2g}$ minority-spin electron transfer between face-sharing $Fe^{2+}$ and $Fe^{3+}$ octahedra. Such an inter-valence charge transfer will have an associated propagation of local lattice distortions,

i.e., polaron motion [20], see Fig 3(a) cartoon of this process. Polaron hopping can be verified from the spectral analysis of Fig. 2(a) as follows.

$^{57}$Fe MS registers a fluctuating valence at each Fe site through which the polaron quasiparticle migrates along <110> octahedral chains of the high pressure *Cc* structure in Fig. S8, similar to Fig. 1(a). Fitting MS spectra in Fig. 2(a) with an appropriate electron-hopping (dynamical) theory yields valence fluctuation rates $\omega = 1/\tau_R$ [16, 19a], e.g., Figs. 2(b) and S11 [10]. Deduced electron hopping rates as a function of pressure are in Fig. 3(a). The thermally activated jump frequency for the polaron arising from the electron transfer process as a function of pressure and temperature is [20a, 21]:

$$\Gamma(T,P) = \frac{1}{\tau_R} = \Gamma_0 \exp\left(-\frac{E_A + PV_A}{k_B T}\right). \qquad (1)$$

In Eq. 1, $E_A$ is activation energy and $V_A$ is activation volume, i.e., changes in energy and volume, respectively, produced by thermal fluctuations for a jump to occur. $\Gamma = 1/\tau_R$ is obtained from fitting spectra at RT, e.g., in Fig. 2(b). The $\Gamma_0$ pre-factor involves electron-transfer distance between neighbouring cations and a characteristic phonon frequency. Although these factors are pressure dependent, they normally only make small (~10 %) corrections to $V_A$ extracted from the slope of a $ln(\Gamma)$ versus $P$ plot, at a fixed temperature [21].

The linearity of the $ln(\Gamma)$ versus $P$ plot in Fig. 3(a) for $P \geq 10$ GPa attests to polaron hopping governed by Eq. (1). Best and worst slopes in Fig. 3(a) in the high pressure regime yield $V_A$ in the range -0.25 to -0.21 cm$^3$.mol$^{-1}$. This small negative $V_A$ value is typical of small polaron hopping in iron oxides [20a, 22].

Polaron hopping is associated with electron transfer across face-sharing octahedra of <110> chains, Fig. S8, similar to those in Fig. 1(a). Such an electron transfer process from cation to cation occurs through an anion intermediary in a two-step process involving highest occupied 3*d* and 2*p* orbitals, $d_i^n p^6 d_j^{n-1} \rightarrow d_i^n p^5 d_j^n \rightarrow d_i^{n-1} p^6 d_j^n$ [23], partially represented in the Fig. 3(a) cartoon. Thus, Fig. 3(a) is compelling evidence of minority-spin electron transfer from the ferrous ion involving the following $Fe^{2+} \rightarrow (OH)^- \rightarrow Fe^{3+}$ and $Fe^{2+} \rightarrow (O) \rightarrow Fe^{3+}$ superexchange pathways.

We suggest a sequence of charge dynamics involving proton delocalization in hydrogen bonds (Fig. 1(d)) influencing electron transfer at cation sites (Fig. 3(a)) in Fe-O–H···O-P configurations, rationalized as follows. The proton in the $(OH)^-$ group ligand contributes a

dipolar field to the Coulombic potential at the Fe site [5, 11]. Proton localisation in one of the potential energy minima along the O–H···O configuration at $P < 10$ GPa, contributes to the Coulombic potential at the Fe site to the extent that the minority-spin electron of $Fe^{2+}$ remains trapped. Here, hydroxyl $(OH)^-$ ligands are on average in a *trans* configuration of $FeO_4(OH)_2$ octahedra. Compression reinforces the hydrogen bond in Fe-O–H···O-P configurations. Protons are then less exclusively associated with ligand nearest-neighbours of Fe, in shared faces of neighbouring octahedra. Such delocalised protons are on average more in centralised regions between oxygens in Fe-O–H–O-P configurations [5]. Thus, dipolar contributions to the Coulombic potential at the Fe sites from $(OH)^-$-group ligands is disrupted, upon the likely advent of proton delocalization onset at 4–7 GPa from signatures in Figs. 1(c) and (d). This furnishes the driving force for 3*d*-electron ($t_{2g}$ minority-spin) delocalization from $Fe^{2+}$ sites. The result then is electron charge transfer and polaron migration to an $Fe^{3+}$ site in a neighbouring face-sharing octahedron along octahedral chains in the structure (see Figs. 1(a) and S8).

Is there any evidence in the Fe MS data that reinforcement of H-bonds and the onset of proton dynamics under pressure affects the electric potential $V$ at proximate cation sites? For this, we turn to the pressure evolution of one of the HI parameters, viz, quadrupole interaction parameter. This manifests in the quadrupole splitting QS of doublet profile signatures for $Fe^{2+}$ and $Fe^{3+}$ valences, seen in spectra at low pressure of Fig. 2. The QS is related to the electric-field-gradient (EFG) at the Fe nuclear site, emanated from asphericity of electronic and lattice charges of its local environment [15]:

$$\mathrm{QS} = \frac{1}{2} eQ\left(V_{zz}\right)\left(1+\frac{\eta^2}{3}\right)^{1/2}. \quad (2)$$

The quadrupole moment is designated by $Q$, $V_{zz} = \partial E/\partial z = \partial^2 V/\partial^2 z$ is the maximum value of the EFG in the principal axes system of the Fe nucleus at the origin and $\eta$ is the asymmetry parameter $0 \le \eta \le 1$, which is zero for an EFG with axial symmetry. The total EFG , $V_{zz}$, has two contributions: from any anisotropic valence electron distribution around the Fe nucleus designated $V_{zz}^{\mathrm{valence}}$ and from more distant ionic charges at neighbouring atoms surrounding the Fe atom in noncubic symmetry, designated $V_{zz}^{\mathrm{lattice}}$. The $V_{zz}^{\mathrm{valence}}$ contribution is by far dominant, from proximity of the valence shell to the Fe nucleus. This is typical for $Fe^{2+}$:$t_{2g}^4 e_g^2$(↑↓↑↑)(↑↑) compared with $Fe^{3+}$:$t_{2g}^3 e_g^2$ (↑↑↑)(↑↑), where in $Fe^{3+}$ with a spherically

symmetric arrangement of valence electronic charge only the smaller $V_{zz}^{lattice}$ contributes to the EFG. More detailed expressions for $V_{zz}$ and $\eta$, involving multiplicative prefactors for $V_{zz}^{lattice}$ and $V_{zz}^{valence}$ include effects of these respective aspherical charge distributions on polarising inner electron shells [15, 24].

QS as a function of pressure is shown in Fig. 3(b) for the two valences. QS for the $Fe^{2+}$ valence, dominated by $V_{zz}^{valence}$, shows small discontinuous changes at ~10 GPa and ~26 GPa. Whereas QS for $Fe^{3+}$, dominated by $V_{zz}^{lattice}$, is nearly constant up to ~10 GPa and then increases monotonically to appreciably higher values. This is a consequence of changing configurations of lattice charge surrounding the cation in $FeO_4(OH)_2$ octahedra, including progressive pressure-induced distortions from cubic symmetry of iron octahedra and delocalization of the proton at hydroxyl group $(OH)^-$ nearest neighbours to Fe. Changes in QS for $Fe^{3+}$ above ~10 GPa cannot be accounted for by changes in axial symmetry, $\eta$ parameter in Eq. (2), as this would increase QS by only ~15% for $\eta$ spanning its full range.

Thus, the behaviour in Fig. 3(b) is suggestive of appreciable changes to the EFG at Fe sites occurring at ~10 GPa onwards from changes in surrounding ligand charge configurations. This includes disruption of covalent O–H bonds from the evolving proton delocalization, onset below 10 GPa, which eventually triggers detrapping of a relatively weakly bound minority-spin electron at $Fe^{2+}$ sites. This picture is in corroboration of polaron hopping and the associated electron-transfer process commencing at ~10 GPa, suggested by activated behaviour in Fig. 3(a).

*Concluding summary.* Pressurization of $(Fe^{2+}Fe^{3+}_2)(PO_4)_2(OH)_2$ mixed-valence barbosalite results in proton delocalization onset in the range 4–7 GPa, involving hydrogen bonds of Fe-O–H···O-P structural segments. This is discerned by IR spectroscopy and pseudo-symmetrization of the lattice parameters. The evolving hydrogen bond reinforcement and proton dynamics impact on the crystal field at proximate Fe cations. This eventually triggers dynamical minority-spin electron exchange along $Fe^{2+} \rightarrow L \rightarrow Fe^{3+}$ pathways (ligand $L$ = O or $(OH)^-$ of shared octahedral faces), evidenced by $^{57}$Fe Mössbauer spectroscopy at 10–30 GPa. The pressure response of these mixed-valence hydroxy phosphates exemplify the interplay between proton (THz) and electron (MHz) dynamics on two disparate time scales in the same condensed phase. This is of widespread relevance to charge dynamics in hydrogen bonded systems (e.g., biomolecular complexes and planetary interiors).

(text incl footnotes 3444 w, figures 549 w, figure captions 481w: **total 4475 w**)

**Acknowledgments**

G.H. acknowledges financial support from the National Research Foundation of South Africa (Grant Number 129291). Financial support for this work was also provided by the joint French-Romanian project ANR-12-IS08-0003, COFeIn.

(text incl footnotes 3444 w, figures 549 w, figure captions 481w: **total 4475 w**)

FIG. 1 Hearne *et. al* SC-XRD and IR

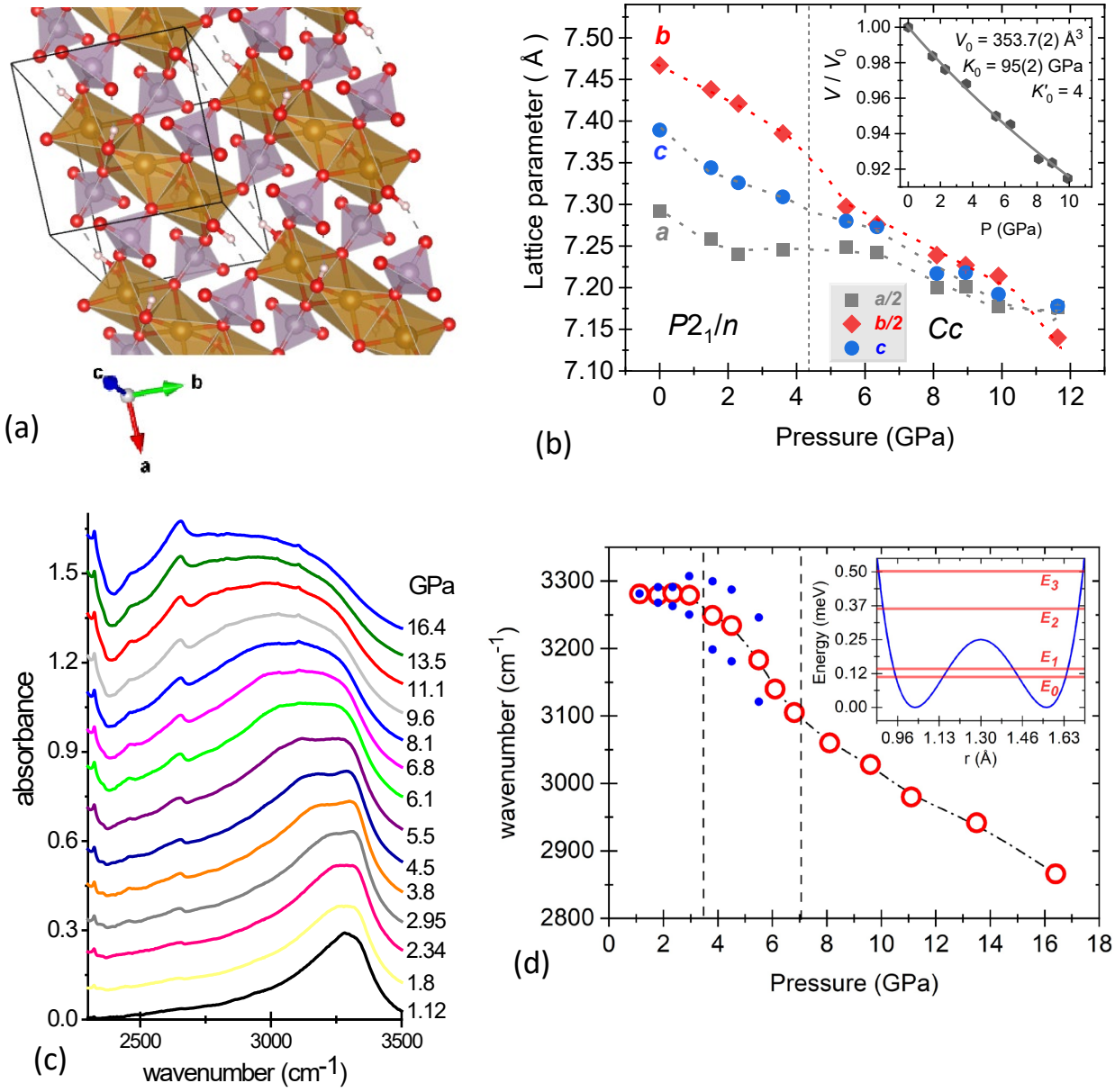


FIG. 1. (a) Face-sharing Fe octahedral chains involving … $Fe^{3+}$–*V*–$Fe^{2+}$–$Fe^{3+}$–$Fe^{3+}$ … sequences, where *V* represents disordered vacant octahedral sites. Hydrogen bonds are depicted by dashed lines in Fe-O–H···O-P structural segments. (b) Lattice parameters as a function of pressure and equation of state (inset). Unit cell relationship: *a*(*Cc*) = 2*a*(*P21/n*), *b*(*Cc*) = 2*b*(*P21/n*), *c*(*Cc*) = *c*(*P21/n*). (c) Pressure evolution of the O–H stretch vibrational profile from the IR probe. (d) Pressure dependence of anti-symmetric and symmetric stretch frequencies at low pressure are shown as solid symbols. Average vibrational frequency is shown as open symbols deduced from extremums in the profiles in (c). Dashed lines delineate where there are changes in pressure dependences. Error bars in (b) and (d), are the size of the symbols. Inset in (d) shows proton potential energy curve for intermediate strength hydrogen bonds O–H···O and lowest lying vibrational energies $E_n$, where a tunnel splitting $E_1 - E_0 = h\nu_p$ is discernible corresponding to THz proton tunnelling frequencies $\nu_p$ [5, 6d, 13].

(text incl footnotes 3444 w, figures 549 w, figure captions 481w: **total 4475 w**)

Fig. 2 Hearne *et. al* MS spectra

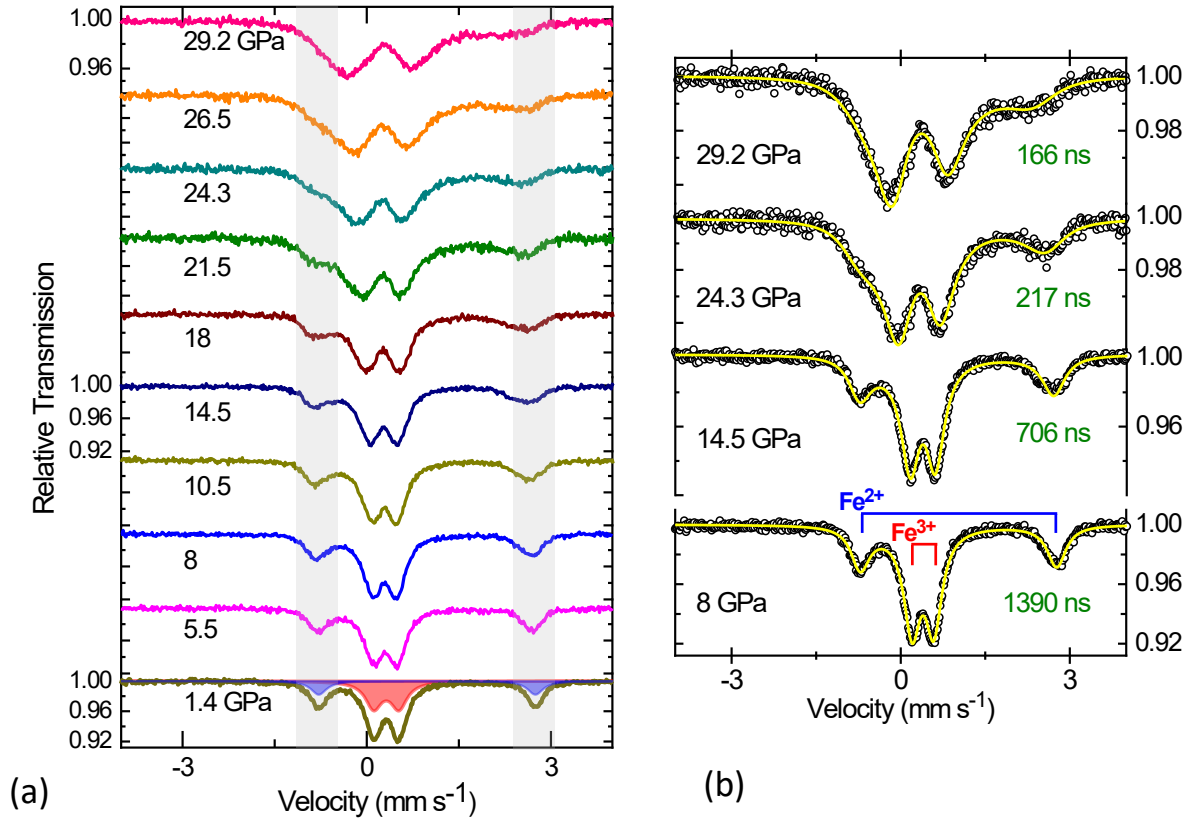


FIG. 2. (a) Mössbauer spectra of $(Fe^{2+}Fe^{3+}_2)(PO_4)_2(OH)_2$, at RT as a function of pressure. At 1.4 GPa, static $Fe^{2+}$ and $Fe^{3+}$ valence signatures are in blue (wide doublet) and red (narrow doublet), respectively, with intensities scaled by 0.5 for clarity. Grey shading highlights $Fe^{2+}$ features becoming progressively asymmetrically broadened beyond ~8 GPa and quite diffuse at ~18 GPa and beyond. (b) Exemplary dynamical theory fitting to some of the Mössbauer spectra in (a). Solid yellow line through data symbols is the overall fit based on a theory of electron transfer (hopping) between neighbouring ferrous and ferric sites leading to $Fe^{2+} \Leftrightarrow Fe^{3+}$ valence fluctuations. Valence fluctuation rates $\omega$ in the range 0.7–7 MHz are derived as a fitting parameter and provide the time interval between electron transfers (relaxation time) $\tau_R = 1/\omega$ indicated in the panels. See Sect. S4 of the SM for further details [10]. Typical spectral doublet parameters of the charge-ordered phase at ambient and low pressures [3a], are depicted by the stick spectra at long electron relaxation times at 8 GPa.

(text incl footnotes 3444 w, figures 549 w, figure captions 481w: **total 4475 w**)

Fig. 3 Hearne *et. al* MS param

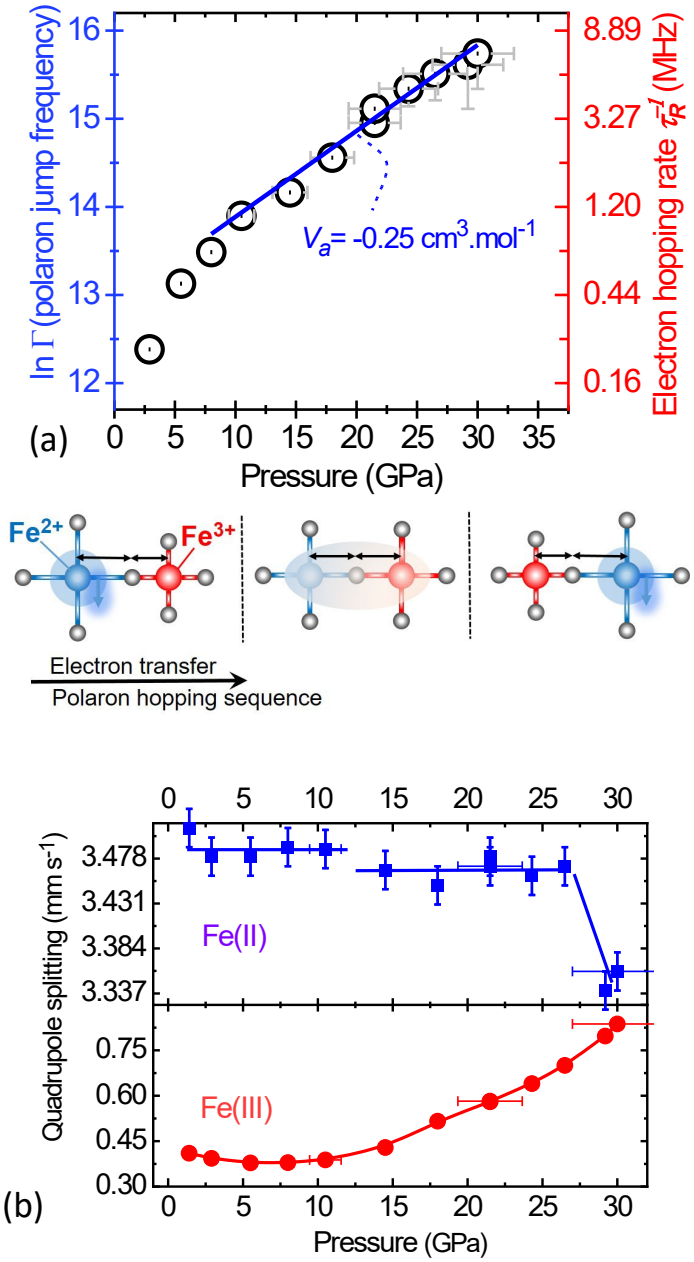


FIG. 3: (a) Linearized plot of polaron jump rate $\Gamma = \frac{1}{\tau_R} \sim \exp\left(-PV_A / k_B T\right)$. Activation volume $V_A$ is obtained from the slope at $P > 10$ GPa, assuming activated-state rate theory is applicable [20a, 21]. Cartoon below the plot depicts polaron hopping and associated bond length changes from delocalization of $t_{2g}$ minority-spin electron ($\uparrow\downarrow\uparrow\uparrow$) between neighbouring sites of $Fe^{2+}$–$Fe^{3+}$ face-sharing octahedra. This leads to a $Fe^{2+} \Leftrightarrow Fe^{3+}$ valence fluctuation rate $\omega = \Gamma = 1/\tau_R$ at an Fe site. Valence fluctuation rates are from fitting Mössbauer spectral line shapes with the appropriate dynamical theory mentioned in the text (Fig. 2(b)). (b) Pressure evolution of the quadrupole splitting QS. Note different scales on the vertical axes. QS parametrizes the electric field gradient at the Fe nucleus from surrounding aspheric electronic and lattice charge distributions. Error bars are discussed in Sect. S4 of the SM [10].

(text incl footnotes 3444 w, figures 549 w, figure captions 481w: **total 4475 w**)

## REFERENCES


[1] J.-M. M. Millet, *FePO Catalysts for the Selective Oxidative Dehydrogenation of Isobutyric Acid into Methacrylic Acid*, Catal. Rev. **40**, 1 (1998).

[2] a) A. K. Padhi, K. S. Nanjundaswamy, and J. B. Goodenough, *Phospho-olivines as positive-electrode materials for rechargeable lithium batteries*, J. Electrochem. Soc. **144**, 1188 (1997); b) P. Sandineni, K. Ghosh, and A. Choudhury, *Electrochemistry of Illusive Barbosalite, $Fe^{2+}Fe_2^{3+}(PO_4)_2(OH)_2$ : An Iron Phosphate Related to Lipscombite Structure*, J. Electrochem. Soc. **166**, A3585 (2019).

[3] a) G. Redhammer, G. Tippelt, G. Roth, W. Lottermoser, and G. Amthauer, *Structure and Mössbauer spectroscopy of barbosalite $Fe^{2+}Fe^{3+2}$ $(PO_4)_2(OH)_2$ between 80 K and 300 K*, Phys. Chem. Miner. **27**, 419 (2000); b) I. Vencato, E. Mattievich, and Y. P. Mascarenhas, *Crystal structure of synthetic lipscombite; a redetermination*, Am. Mineral. **74**, 456 (1989).

[4] O-H···O hydrogen bonds have been classified as weak , intermediate and strong according to the bond length constituted by the distance $R$ between the oxygens; $R > 2.6$ Å ('weak'), 2. 4 Å $< R <$ 2.6 Å ('intermediate'), $R <$ 2.4 Å ('strong') in the contemporary literature. Weak hydrogen bonds involve a high proton potential energy barrier and the protons are localised in an asymmetric O-H···O configuration. Moderate or intermediate strength bonds have a low barrier, comparable to the zero point energy, where quantum tunnelling across the barrier and the advent of proton delocalization is possible. Strong hydrogen bonds involve a highly anharmonic single minimum potential and there is proton localization again in symmetric covalent O-H-O configurations.

[5] Y. Li, S. M. Winter, and R. Valentí, *Role of Hydrogen in the Spin-Orbital-Entangled Quantum Liquid Candidate $H_3LiIr_2O_6$*, Phys. Rev. Lett. **121**, 247202 (2018).

[6] a) D. Marx, *Proton transfer 200 years after von Grotthuss: Insights from ab initio simulations*, ChemPhysChem **7**, 1848 (2006); b) T. Meier, S. Petitgirard, S. Khandarkhaeva, and L. Dubrovinsky, *Observation of nuclear quantum effects and hydrogen bond symmetrisation in high pressure ice*, Nat. Commun. **9**, 2766 (2018); c) P. Johannsen, *Vibrational states and optical transitions in hydrogen bonds*, J. Phys.: Condens. Matter **10**, 2241 (1998); d) R. H. McKenzie, C. Bekker, B. Athokpam, and S. G. Ramesh, *Effect of quantum nuclear motion on hydrogen bonding*, J. Chem. Phys. **140**, 174508 (2014).

[7] a) M. Benoit, D. Marx, and M. Parrinello, *Tunnelling and zero-point motion in high-pressure ice*, Nature **392**, 258 (1998); b) W. Holzapfel, *On the symmetry of the hydrogen bonds in ice VII*, J. Chem. Phys. **56**, 712 (1972); c) L. Lin, J. A. Morrone, and R. Car, *Correlated tunneling in hydrogen bonds*, J. Stat. Phys. **145**, 365 (2011).

[8] a) S. D. Jacobsen, *Effect of Water on the Equation of State of Nominally Anhydrous Minerals*, Rev. Mineral. Geochem. **62**, 321 (2006); b) M. Hou, Y. He, B. G. Jang, S. Sun, Y. Zhuang, et al., *Superionic iron oxide–hydroxide in Earth's deep mantle*, Nat. Geosci. **14**, 174 (2021).

(text incl footnotes 3444 w, figures 549 w, figure captions 481w: **total 4475 w**)


[9] G. R. Hearne, W. N. Sibanda, E. Carleschi, V. Pischedda, and J. P. Attfield, *Pressure-induced suppression of charge order and nanosecond valence dynamics in $Fe_2OBO_3$*, Phys. Rev. B **86**, 195134 (2012).

[10] See Supplemental Material at http://XXXXXXXXX for experimental methodology details, structural data and analysis from SC-XRD and DFT calculations, further IR data and DFT calculations, details on Mössbauer spectral analysis and simulations related to Fe valence fluctuations. Also included are crystallographic information files (CIFs) for all structures depicted in the manuscript and SM.

[11] a) M. Pasternak, A. Milner, G. K. Rozenberg, R. Taylor, and R. Jeanloz, *Pressure Induced Self-Oxidation of $Fe(OH_2)$*, Phys. Rev. Lett. **92**, 085506 (2004); b) S. Speziale, R. Jeanloz, A. Milner, M. P. Pasternak, and J. M. Zaug, *Vibrational spectroscopy of $Fe(OH)_2$ at high pressure: Behavior of the OH bond*, Phys. Rev. B **71**, 184106 (2005).

[12] P. Johannsen, V. Schäferjohann, and S. Kapphan, *Effect of pressure on OH and OD impurities in $LiNbO_3$*, J. Phys.: Condens. Matter **11**, 583 (1999).

[13] In the case of weak hydrogen bonds, where there are asymmetric O-H···O configurations, lowest $E_0$ and $E_1$ energies as well as excited state $E_2$ and $E_3$ energies are degenerate vibrational states well below the proton potential-energy barrier height of ~1 eV . Their splittings become discernible on the scale of the barrier height, when the vibrational energies are comparable to the barrier height (intermediate strength hydrogen bonds).

[14] The hyperfine interaction (HI) parameters as well as Fe site abundances are derived from fitting the spectral envelope with an appropriate static (Lorentzian sub-components) or dynamical theory. The isomer (chemical) shift IS is proportional to the *s*-electron density at the Fe nucleus and is influenced by *3d*-electron shielding. The quadrupole doublet-splitting, QS, is proportional to the aspherical distribution of surrounding electronic and nearest neighbor atomic charge. The IS, QS, and $H_{hf}$ (from magnetically split hyperfine structure) parameters have distinct "fingerprint" values for both valences and spin states of $Fe^{2+}(3d^6)$ and $Fe^{3+}(3d^5)$.

[15] P. Gütlich, E. Bill, and A. X. Trautwein, *Mössbauer Spectroscopy and Transition Metal Chemistry: Fundamentals and Applications* (Springer, Berlin, 2011).

[16] R. H. Herber and H. Eckert, *Electron hopping in FeOCl intercalation compounds: A Mössbauer relaxation study*, Phys. Rev. B **31**, 34 (1985).

[17] QS hyperfine interaction signatures will be observed provided that a complete precession of the quadrupole moment takes place before the $^{57}Fe$ nucleus de-excites to a ground state, i.e., $\tau_Q < \tau_N$ , where $\tau_N = 140$ ns is the lifetime of the nuclear excited state . Quadrupole precession frequency $\omega_Q = (½)(eQV_{zz})/\hbar$ , where $V_{zz}$ is the maximum value of the electric field gradient and $Q$ the quadrupole moment. The numerator is the quadrupole (spectral doublet) splitting QS in the static limit for an axially symmetric EFG. The quadrupole precession frequency is $\omega_Q \sim 14 \times 10^7$ rad $s^{-1}$ for QS ~ 2 mm $s^{-1}$ and thus the corresponding precession time is $\tau_Q \sim 40$ ns. Similar arguments hold for the magnetic hyperfine interaction where the more well known Larmor precession frequency of the nuclear magnetic moment would be the main consideration.

(text incl footnotes 3444 w, figures 549 w, figure captions 481w: **total 4475 w**)


[18] B. Ellis, L. K. Perry, D. H. Ryan, and L. Nazar, *Small polaron hopping in $Li_xFePO4$ solid solutions: coupled lithium-ion and electron mobility*, J. Am. Chem. Soc. **128**, 11416 (2006).

[19] a) For example MossWinn 4.0, Mössbauer spectral analysis software, by Zoltán Klencsár (see http://www.mosswinn.com/); b) M. Blume, *Stochastic theory of line shape: generalization of the Kubo-Anderson model*, Phys. Rev. **174**, 351 (1968).

[20] a) A. Goddat, J. Peyronneau, and J. Poirier, *Dependence on pressure of conduction by hopping of small polarons in minerals of the Earth's lower mantle*, Phys. Chem. Miner. **27**, 81 (1999); b) Y. Natanzon, A. Azulay, and Y. Amouyal, *Evaluation of Polaron Transport in Solids from First-principles*, Isr. J. Chem. **60**, 768 (2020).

[21] S. J. Tracy, L. Mauger, H. Tan, J. A. Munoz, Y. Xiao, et al., *Polaron-ion correlations in $Li_xFePO_4$ studied by x-ray nuclear resonant forward scattering at elevated pressure and temperature*, Phys. Rev. B **90**, 094303 (2014).

[22] The value of $V_A$ for small polaron hopping should be of the order of the difference in atomic volumes of $Fe^{3+}$ and $Fe^{2+}$ ions, $\Delta V$ = -0.23 $cm^3$ $mol^{-1}$, corresponding to the propagation of local lattice distortions depicted in Fig. 3(a).

[23] D. I. Khomskii, *Transition metal compounds* (Cambridge University Press, Cambridge, United Kingdom, 2014).

[24] M. Grodzicki, G. Redhammer, G. Amthauer, V. Schunemann, A. Trautwein, et al., *Electronic structure of Fe-bearing lazulites*, Am. Mineral. **88**, 481 (2003).